ACTA ACUSTICA UNITED WITH ACUSTICA
Vol. 95 (2009) 189 – 202

DOI 10.3813/AAA.918143

An Iterative Method for the Interaction Between a Bounded Beam and an Interface Defect in Solids, Under Kirchhoff Approximation

Nacera Bedrici[1,2,3], Philippe Gatignol[1], Catherine Potel[2,3]

[1)] Laboratoire Roberval, UMR CNRS 6253, Université de Technologie de Compiègne, BP 20 529, 60205 Compiègne Cedex, France.
[2)] Laboratoire d'Acoustique de l'Université du Maine, UMR CNRS 6613, Avenue Olivier Messiaen, 72 085 LE MANS, France. Catherine.Potel@univ-lemans.fr
[3)] Fédération Acoustique du Nord-Ouest, (FANO) FR CNRS 3110, France

Summary
The method of passive re-emission under Kirchhoff approximation is used in this paper in order to solve the problem of the interaction of a monochromatic ultrasonic bounded beam (emitted by a plane transducer) with a bi-dimensional structure fluid/solid/solid which includes a plane defect located at the plane interface separating the two solids (assumed to be isotropic). The ultrasonic beam is decomposed into plane waves, using Fourier transforms. The presence of both the interfaces and the defect produces successive reflections. In order to take into account all the corresponding fields, an iterative method has been implemented. At each iteration, the problem of the scattering by the defect is processed with the passive re- emission method, the data on the defect being calculated under Kirchhoff approximation (in good agreement with the Geometrical Theory of Diffraction for a defect located in a fluid medium); the transmission through the interfaces is performed for plane waves, the scattered field being expressed using Fourier integrals. This iterative method gives a more accurate solution than the global one, namely the passive re-emission principle under Kirchhoff approximation straightforwardly applied on the whole system of the structure. Numerical results are given (cartographies and cuts of the pressure field in the fluid), which show -i) the effect of the defect on the field which propagates in the structure, -ii) the convergence rate of the iterative process as a function of the incident angle, -iii) the changes in the field depending on the location of the defect.

PACS no. 43.20.-f, 43.20.El, 43.20.Fn, 43.35.-c, 43.35.Cg, 43.35.Zc

1. Introduction

Multilayered media such as composite structures are increasingly used in industries due to their mechanical properties for a given weight. Different kind of defects (cracks, delaminations, ...) can appear during the production process and during the entire life of the structure, and their detection is crucial. In the general framework of ultrasonic non destructive testing, modeling the interaction of an ultrasonic bounded beam with a finite size heterogeneity set in a structure is a difficult task [1]. The scattering of ultrasonic waves by a crack located near or on the free surface of a structure has been studied by several authors [2, 3, 4, 5, 6, 7]. As far as heterogeneities at interfaces are concerned, the first contributions for solid/solid interfaces are dedicated to two-dimensional geometries and to incident plane waves: Boström [8] and Chevalier *et al.* [9] for incident SH-waves, Wang *et al.* [10] for layered media and Qu [11] for the in-plane case. Previously, Srivastava *et al.* [12] gave a solution for a tri-dimensional configuration with a longitudinal wave at normal incidence. In 1991, Boström *et al.* [13, 14] used the integral equation method to solve the problem of scattering of a plane wave by a tridimensional defect in fluid media. The bonding between two media is also the subject of numerous studies, especially in multilayered media, from both a theoretical and an experimental point of view. Among these studies, notably, Baltazar *et al.* [15, 16, 17] and Rokhlin *et al.* [18] widely investigated the characterization of adhesive layers and the evaluation of interface behaviors. More recently, Shkerdin *et al.* [19] investigated the case of the interaction of Lamb modes with delaminations between two isotropic absorbing materials, using a modal decomposition.

Most of these contributions are concerned with incident plane waves, with integral equation techniques to solve the scattering problem, leading therefore to intricate analysis. The present work aims at studying the interaction between an incident beam with an internal finite defect, us-

Received 4 September 2008,
accepted 12 November 2008.

ing the plane wave Fourier decomposition. The analysis of the wave scattering from defect is simplified by introducing the Kirchhoff approximation. The method is presented here for a very simple "academic" situation in order to emphasize clearly its advantages (compared to the numerical methods currently in use): rapidity (less than one minute for obtaining the acoustic field in a spatial domain, even for the highest frequency range), tractability (no huge matrices like in a finite element method), and possibility to extent the method to multiple defects and to several interfaces.

More precisely, the aim of this paper is to study, using Kirchhoff approximation and an iterative method, the interaction of a monochromatic ultrasonic bounded beam with *a fluid / isotropic solid / isotropic solid* structure including a finite length defect, and to obtain the reflected and transmitted fields (Figure 1). The fluid medium labelled "0" and the solid labelled "2" set respectively above and below the solid layer labelled "1" are semi-infinite. The geometry of the problem is a two-dimensional one. The sagittal plane is denoted (O, x, z), the z-axis being perpendicular to the interfaces (denoted I and II), and θ is the angle between the z-axis and the acoustic axis of the emitting transducer (diameter $2a$, frequency $f = \omega/(2\pi)$). The solid layer 1 (thickness denoted h_1) and the semi-infinite solid 2 are perfectly bonded all along their common interface II, except on a $2L$-length delamination-type defect.

The decomposition of bounded beams into monochromatic plane waves, used in order to describe their interaction with plane layered structures, is first briefly described in section 1, and then it is shown how acoustic field cartographies may be easily obtained. The general principle of Kirchhoff approximation is then explained in section 2 from considering the elementary problem of the interaction of a plane wave with an interface including a finite size defect. Finally in section 3, the implementation of the iterative method under Kirchhoff approximation is performed on a fluid/solid/solid structure (Figure 1), and several specific results are presented.

Nomenclature of subscripts and superscripts

Superscripts:
(i): infinite defect on interface.
(h): healthy interface.
(k): Kirchhoff approximation.
(s): scattered field under Kirchhoff approximation.
n: number of iteration (number of times that the field comes across the defect).

Subscripts:
e: emitter.
a: waves propagating towards $z > 0$.
b: waves propagating towards $z < 0$.
x, z: component on x, z-axis.
inc: incident field (in fluid medium 0).
α: considered medium, $\alpha = 0, 1, 2$.
η: $\eta = L$ for longitudinal (pressure) wave and $\eta = T$ for transversal (shear) wave.

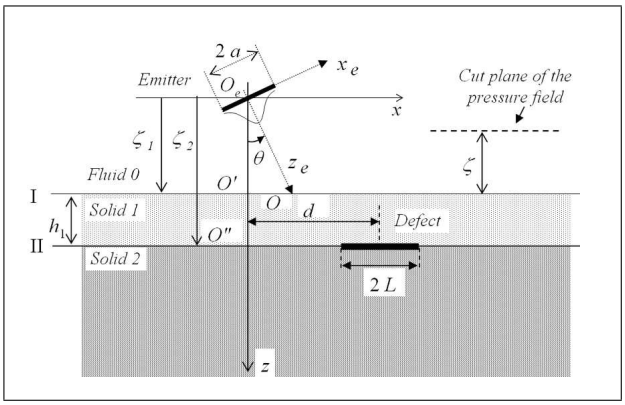

Figure 1. Geometry of the problem.

Examples:
$\boldsymbol{u}_{1b}^{(s)}$: scattered field propagating towards $z<0$ in medium 1.
$u_{1za}^{(h)}$: z-component of the field $\boldsymbol{u}_{1a}^{(h)}$, i.e. the field propagating towards $z > 0$ in medium 1 for a structure with a healthy surface.
$\boldsymbol{u}_{1b}^{2(k)}$: 2nd iteration of the approximated field (under Kirchhoff approximation) propagating towards $z < 0$ in medium 1.
$u_{2za_T}^{1(i)}$: z-component of the field $\boldsymbol{u}_{2a_T}^{1(i)}$, i.e. the first iteration of the transversal field propagating towards $z > 0$ in medium 2 for a structure with an infinite defect.

2. Interaction of an ultrasonic beam with homogeneous plane interfaces

The implementation of Kirchhoff approximation, with a bounded beam as an incident field, needs first of all to solve some elementary problems: the decomposition of the bounded beam into monochromatic plane waves (section 2.1), the interaction of a plane wave with a homogeneous plane interface separating two isotropic solid media with various boundary conditions (section 2.2), and, finally, the interaction of the bounded beam with plane interfaces (section 2.3). The method used here to compute the Fourier integrals which lead to cartographies of the acoustic fields, is particularly fast because i tavoids many constraints of the FFT algorithm (see section 2.3.3).

2.1. Principle of the decomposition of a monochromatic beam into plane waves

The principle of the decomposition of a monochromatic beam into plane waves (or angular spectrum decomposition), based on the linearity of the field equations, is a very well-known principle which can be applied to a scalar or a vectorial field function [20, 21, 22, 23, 24, 25, 26, 27, 28, 29, 30, 31, 32, 33, 34]. Here, the incident displacement field $\boldsymbol{u}_{0inc}$ is built, at any point $M(x_e, z_e)$ of the half-space $z_e > 0$, as a superposition (with the parameter k_{x_e}) of all the plane and evanescent waves (the $\exp(-\mathrm{i}\omega t)$ factor being omitted):

$$u_{0inc}(x_e, z_e) = \int_{-\infty}^{+\infty} A_e(k_{x_e}) \frac{k_0(k_{x_e})}{k_0} \cdot \exp\left[\mathrm{i}(k_{x_e} x_e + k_{0z_e} z_e)\right] \mathrm{d}k_{x_e}, \quad (1)$$

where $A_e(k_{x_e})$ is the amplitude of each plane wave and where $(k_{x_e}, 0, k_{0x_e})$ are the components of the corresponding wave vector $\boldsymbol{k}_0$ in the fluid 0 (angular frequency ω) in the coordinate system $R_e = (O_e, x_e, y_e, z_e)$ linked to the emitting transducer (Figure 1). These components are such as (dispersion relation)

$$(k_{x_e})^2 + (k_{0z_e})^2 = ||\boldsymbol{k}_0||^2 = (k_0)^2 = (\omega/V_0)^2, \quad (2)$$

where V_0 is the speed of the waves propagating in the fluid 0. The determination of k_{0z_e}, as a function of k_{x_e}, is chosen in order to ensure the radiation condition of the field in the half-space considered.

The z-component of particle displacement $u_{0z_e,inc}(x_e, 0)$ in the fluid, normal to the front face of the emitting transducer, is supposed to be known, and can arise from experimental results or from an analytical expression. For of a Gaussian beam, it takes the following form,

$$u_{0z_e,inc}(x_e, 0) = U_0 \exp\left[-(x_e/a)^2\right], \quad (3)$$

where a is the nominal radius of the emitter.

Using equation (1), the displacement $u_{0z_e,inc}(x_e, 0)$ can be written as

$$u_{0z_e,inc}(x_e, 0) = \int_{-\infty}^{+\infty} A_e(k_{x_e}) \frac{k_{0z_e}}{k_0} \exp\left[\mathrm{i}k_{x_e} x_e\right] \mathrm{d}k_{x_e}, \quad (4)$$

which permits, by means of an inverse Fourier transform, to obtain the angular spectrum

$$A_e(k_{x_e}) \frac{k_{0z_e}}{k_0} = \frac{1}{2\pi} \int_{-\infty}^{+\infty} u_{0z_e,inc}(x_e, 0) \exp\left[-\mathrm{i}k_{x_e} x_e\right] \mathrm{d}x_e, \quad (5)$$

and thus the amplitude $A_e(k_{x_e})$ of each incident plane wave which is therefore known. The incident displacement field $\boldsymbol{u}_{0inc}$ can thus be determined in the whole half-space through the calculation of Fourier integral (1).

It should be noted that the phases of the complex amplitudes $A_e(k_{x_e})$ determined by equation (5) are referenced at the point O_e.

2.2. Interaction of a plane wave with a homogeneous plane interface: boundary conditions and reflection/transmission problem

2.2.1. Plane waves in an isotropic elastic medium

The formalism used here to describe the propagation in an isotropic elastic medium (denoted by the subscript α) is the classical one [35, 36]. In particular, the displacement vector $\boldsymbol{U}_{\alpha_\eta}$ of each plane wave (η) has the following form:

$$\boldsymbol{U}_{\alpha_\eta}(x, z; t) = X_{\alpha_\eta} \boldsymbol{P}_{\alpha_\eta} \exp\left[\mathrm{i}\left(k_x x + k_{\alpha z_\eta} - \omega t\right)\right], \quad (6)$$

X_{α_η} and $\boldsymbol{P}_{\alpha_\eta}$ being respectively the amplitude and the polarization vector of the wave (η), where $\eta = L$ and $\eta = T$ respectively for longitudinal (pressure) wave and transversal (shear) waves, and where $X = A$ for waves which propagate (or decrease) in the direction $z > 0$ and $X = B$ for those which propagate (or decrease) in the direction $z < 0$.

Using the Hooke law in the isotropic solid medium α, the stress vector $\boldsymbol{T}_{\alpha_\eta}$ (associated to the normal $\boldsymbol{e}_z$ to the interfaces) of each plane wave (η) has the following form:

$$\boldsymbol{T}_{\alpha_\eta} = T_{\alpha x z_\eta} \boldsymbol{e}_x + T_{\alpha z z_\eta} \boldsymbol{e}_z, \quad (7)$$

where the components of the stress tensor are given by

$$T_{\alpha x z_\eta} = \mu_\alpha \left(\frac{\partial U_{\alpha x_\eta}}{\partial z} + \frac{\partial U_{\alpha z_\eta}}{\partial x} \right), \quad (8a)$$

$$T_{\alpha z z_\eta} = \left(\lambda_\alpha + 2\mu_\alpha\right) \frac{\partial U_{\alpha z_\eta}}{\partial z} + \lambda_\alpha \frac{\partial U_{\alpha x_\eta}}{\partial x}, \quad (8b)$$

with λ_α and μ_α the Lamé coefficients of the isotropic medium α.

It will be subsequently useful to identify in each medium the waves which propagate (or decrease) in the direction $z > 0$ (denoted "a") and those which propagate (or decrease) in the direction $z < 0$ (denoted "b"). This (classical) identification can be summarized as

field "a", $\eta = L, T$ (9a)

$$\begin{cases} k_{\alpha z_\eta} > 0 & \text{for propagative waves,} \\ k''_{\alpha z_\eta} > 0 & \text{for evanescent waves,} \end{cases}$$

field "b", $\eta = L, T$ (9b)

$$\begin{cases} k_{\alpha z_\eta} < 0 & \text{for propagative waves,} \\ k''_{\alpha z_\eta} < 0 & \text{for evanescent waves,} \end{cases}$$

with $k_{\alpha z_\eta} = \mathrm{i}k''_{\alpha z_\eta}$ when the waves are evanescent.

2.2.2. Boundary conditions, including bonding conditions

In the following, a homogeneous interface or part of an interface, means that the physical conditions to be satisfied on both sides of the surface separating two media (here, the healthy interface or the finite defect) do not depend on the coordinate(s) along it. In practice, it is assumed that the internal interface between solids 1 and 2 fulfills a perfect adhesion between the two media, whereas the finite defect yields a delamination or a partial bonding (with constant characteristics of the glue).

For a perfect (rigid) bonding between the two solids 1 and 2 at the plane interface II (see Figure 1), the boundary conditions express the continuity of the displacement and stress vectors (associated to the normal $\boldsymbol{e}_z$ to the interface), i.e.

$$\boldsymbol{U}_1(x, z = \zeta_2; t) = \boldsymbol{U}_2(x, z = \zeta_2; t), \quad \forall x, z = \zeta_2, \forall t, \quad (10a)$$

$$\boldsymbol{T}_1(x, z = \zeta_2; t) = \boldsymbol{T}_2(x, z = \zeta_2; t), \quad \forall x, z = \zeta_2, \forall t. \quad (10b)$$

Conditions (10) are those involved in the preliminary problem solved for a healthy interface II (see section 4.1.2).

For a total delamination on the interface II, the boundary conditions express that the stress vector vanishes, i.e.

$$\boldsymbol{T}_1(x, z = \zeta_2; t) = 0, \quad z = \zeta_2, \forall t, \tag{11a}$$
$$\boldsymbol{T}_2(x, z = \zeta_2; t) = 0, \quad z = \zeta_2, \forall t, \tag{11b}$$

for all the values of x corresponding to points on the defect.

Intermediate (elastic) bonding between solid media 1 and 2 at the interface II can also be considered, using the boundary conditions introduced in 1990 by Pilarski *et al.* [37] and widely used from that time.

In the situation considered in this paper, conditions (11) are associated to defects of finite extent (on the interface II). But, in order to solve the preliminary problem these conditions (11) are extended all along interface II (infinite defect on interface II, see section 4),

2.2.3. Reflection/transmission problem for plane waves

Generally speaking, the interaction of an oblique incident monochromatic plane wave (angular frequency ω) polarized in the plane (O, x, z) and propagating in this plane, with a plane interface separating two isotropic semi-infinite media 1 and 2 generates two waves in each solid α ($\alpha = 1, 2$): a longitudinal and a transversal vertical wave (labeled respectively by $\eta = L$ and $\eta = T$), with associated wave numbers denoted respectively k_{α_L} and k_{α_T}. Given the properties of the incident (longitudinal or transversal vertical) wave (especially its displacement amplitude), the boundary conditions (10) or (11) lead to four equations with four unknowns X_{α_η} ($\alpha = 1, 2, \eta_L, T$).

2.3. Interaction of a bounded beam with a plane layered structure

2.3.1. Change of coordinate system

Once the bounded incident field $\boldsymbol{u}_{0,inc}$ has been decomposed into monochromatic plane waves, at any point $M(x_e, z_e)$, $z_e > 0$, in the coordinate system R_e (see section 2.1), it is useful to change the coordinate system in order to study the interaction of each monochromatic plane wave with the structure. The new coordinate system $R = (O_e, x, y, z)$ has its plane $z = 0$ parallel to the interface I and located at a distance ζ_1 from it, and is deduced from R_e by a rotation of angle θ around the y-axis (θ being the incident angle of the acoustic beam, see Figure 1). The coordinates of a given point M in this new coordinate system are denoted $M(x, 0, z)$ and the components of each wave vector $\boldsymbol{k}_0$ are denoted $(k_x, 0, k_{0z})$, where the component k_x has no subscript associated to a medium, because, due to the boundary conditions written for any given x, this component is the same in each medium. These components depend on k_{x_e} through the dispersion equation (2) and through the usual relations,

$$k_x = k_{x_e} \cos\theta + k_{0z_e} \sin\theta, \tag{12a}$$
$$k_{0z} = -k_{x_e} \sin\theta + k_{0z_e} \cos\theta. \tag{12b}$$

It should be noted that the invariance of the dot product

$$\boldsymbol{k}_0 \cdot \boldsymbol{O_e M} = k_{x_e} x_e + k_{0z_e} z_e = k_x x + k_{0z} z \tag{13}$$

leads to the following expression for the incident particle displacement $\boldsymbol{u}_{0,inc}$ in the fluid 0, in the coordinate system R

$$\boldsymbol{u}_{0,inc}(x, z) = \int_{-\infty}^{+\infty} A_e(k_{x_e}) \frac{\boldsymbol{k}_{0x_e}}{k_0} \cdot \exp\left[\mathrm{i}\left(k_x x + k_{0z} z\right)\right] \mathrm{d}k_{x_e}, \tag{14}$$

i.e.

$$\boldsymbol{u}_{0,inc}(x, z) = \int_{-\infty}^{+\infty} A'_e(k_{x_e}) \frac{\boldsymbol{k}_{0x_e}}{k_0} \cdot \exp\left[\mathrm{i}k_{0z}\left(z - \zeta_1\right)\right] \exp\left(\mathrm{i}k_x x\right) \mathrm{d}k_{x_e}, \tag{15}$$

with

$$A'_e(k_{x_e}) = A_e(k_{x_e}) \exp\left(\mathrm{i}k_{0z}\zeta_1\right). \tag{16}$$

It is worth noting that, as it has been mentioned just after equation (5), the amplitudes $A_e(k_{x_e})$ are referenced at the point O_e. In the same way, the amplitudes $A'_e(k_{x_e})$ are referenced at the point O' (see Figure 1).

2.3.2. Interaction of the incident beam with a healthy structure fluid 0/solid 1/solid 2

The aim of this Section is to show, for a healthy structure, how it is possible to reconstruct the different displacement fields in each medium, using a global method involving Fourier transforms. However, it would have been also possible to use an iterative method, such as that used in section 4 in the frame of Kirchhoff approximation. In the case of a healthy structure, it may be shown that the successive displacement fields in the fluid, corresponding to the successive reflections on each interface, constitute a convergent geometric series: at each step, the magnitude of outgoing field in the fluid is smaller than that of the outgoing field at the previous step, and thus, because the ratio between these fields is the same at each step, the total field is the sum of a convergent geometric series and this sum is equal to the solution obtained by the present global method.

The interaction of each monochromatic plane wave of the incident beam with the structure fluid 0/solid 1/solid 2 (Figure 1) can then be classically studied by writing the boundary conditions at each interface, which leads to *seven scalar equations* written as follows (using notations defined in section 2.2.2):

– three equations coming from the continuity of the z-component of the displacement vector $\boldsymbol{U}$ and from the continuity of the stress vector $\boldsymbol{T}$ at interface I (fluid 0/solid 1), namely

$$U_{0z}(x, z = \zeta_1; t) = U_{1z}(x, z = \zeta_1; t), \quad \forall x, z = \zeta_1, \forall t, \tag{17a}$$
$$\boldsymbol{T}_0(x, z = \zeta_1; t) = \boldsymbol{T}_1(x, z = \zeta_1; t), \quad \forall x, z = \zeta_1, \forall t, \tag{17b}$$

– four equations coming from the boundary conditions (10) or (11) at interface II (solid 1 / solid 2), whether this interface is healthy or not (with an infinite defect).

Seven unknown amplitudes are solutions of these seven boundary conditions: the amplitude $\boldsymbol{B}_0$ of the wave reflected in fluid 0, the four amplitudes $\boldsymbol{A}_{1L}$, $\boldsymbol{A}_{1T}$, $\boldsymbol{B}_{1L}$, $\boldsymbol{B}_{1T}$,

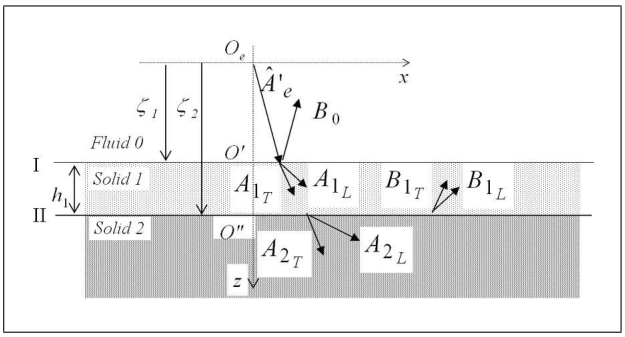

Figure 2. The reflection/transmission problem for each plane wave constituting the incident beam.

of the waves propagating or decreasing in solid layer 1, and the two amplitudes A_{2L}, A_{2T}, of the waves transmitted in solid 2 (figure 2), where a radiation condition is applied.

It should be noted that, the phases of the displacement amplitudes of each wave are referenced at the interface from which they are generated: the amplitudes A'_e, B_0, A_{1L} and A_{1T} are referenced at the point O', whereas the amplitudes B_{1L}, B_{1T}, A_{2L} and A_{2T} are referenced at point O'' (see Figure 2).

The reflected field in fluid 0 can then be reconstructed, taking the form of a Fourier integral as

$$\boldsymbol{u}_{0,b}(x,z) = \int_{-\infty}^{+\infty} R_0 A'_e(k_{x_e}) \boldsymbol{P}_{0b} \cdot \exp\left\{\mathrm{i}\left[k_x x - k_{0z}\left(z-\zeta_1\right)\right]\right\} \mathrm{d}k_{x_e}, \tag{18}$$

where $\boldsymbol{P}_{0b}$ and R_0 are respectively the polarization vector of the reflected wave in fluid 0 and the reflection coefficient obtained from the resolution of the 7th-order linear system above-mentioned ($R_0 = B_0/A'_e$).

Similar equations can be written for the fields in the solids 1 and 2,

$$\boldsymbol{u}_1(x,z) = \sum_{\eta=L,T} \int_{-\infty}^{+\infty} \Big\{ A_{1_\eta} \boldsymbol{P}_{1a_\eta} \cdot \exp\left[\mathrm{i}k_{1z_\eta}\left(z-\zeta_1\right)\right] + B_{1_\eta} \boldsymbol{P}_{1b_\eta} \cdot \exp\left[-\mathrm{i}k_{1z_\eta}\left(z-\zeta_2\right)\right] \Big\} \exp\left(\mathrm{i}k_x x\right) \mathrm{d}k_{x_e} \tag{19}$$

and

$$\boldsymbol{u}_2(x,z) = \sum_{\eta=L,T} \int_{-\infty}^{+\infty} A_{2_\eta} \boldsymbol{P}_{2a_\eta} \cdot \exp\left[\mathrm{i}k_{2z_\eta}\left(z-\zeta_2\right)\right] \exp\left(\mathrm{i}k_x x\right) \mathrm{d}k_{x_e}, \tag{20}$$

the amplitudes A_{1_η}, B_{1_η} and A_{2_η}, $\eta = L, T$, being deduced from the previous linear system of seven equations.

2.3.3. Implementation of the method

This Section aims at giving some explanations about the computation method used in order to easily visualize the acoustic fields in the different media either in the form of cartographies linked to the structure (i.e. linked to the coordinate system (O, x, z)), or through cuts of the acoustic fields in a plane parallel to the structure (thus for a given z). In these computations, it appears easier to use the space variables (x, z) in the exponential factors of the different Fourier integrals and to choose a set of values for the parameter x (eventually with a constant step sampling), and to use either a single value for z (for a cut) or a set of values for z (possibly with a constant step sampling) for a cartography. All these Fourier integrals have the form

$$I = \int_{-\infty}^{+\infty} R(k_x)\, A(k_{x_e}) \exp\left[\mathrm{i}\left(k_x x + k_z z\right)\right] \mathrm{d}k_{x_e}, \tag{21}$$

where k_x and k_z are functions of k_{x_e}.

Instead of using a Fast Fourier Transform (FFT) algorithm in order to calculate the integral (21), it is much easier to calculate it straightforwardly, using a simple classical trapezoid method, on the basis of the initial sampling used for k_{x_e} (and using the invariance of the dot product $\boldsymbol{k}_0 \cdot \boldsymbol{O_eM}$ mentioned in section 2.3.1.). Note that the use of the FFT algorithm would need to change the integration variable from k_{x_e} into k_x, with the introduction of a Jacobian and an interpolation technique in order to calculate the relevant values of the amplitudes . Moreover, due to the factorization properties of the exponential function, a matrix computation, using for example MATLAB® or SCILAB softwares, permits to calculate all the Fourier integrals by trapezoid method in a single step. Note also that there is no constraint linking the integration variable and the space variable (where the field is calculated), neither for the values, nor for the sampling.

Table I. Characteristics of each medium of the structure, where $k_0 a$ and $k_{\alpha_\eta} a$, $\eta = L, T$, $\alpha = 0, 1, 2$ are respectively the adimensional wave numbers for pressure waves in fluid 0 and for longitudinal ($\eta = L$) and shear ($\eta = T$) waves in solid α. The radius of the emitter, the thickness of layer 1 and the density of each medium α are respectively denoted a, h_1 and ρ_α.

Fluid 0	$k_0 a = 100$
Solid 1	$k_{1_L} a = 40$, $k_{1_T} a = 80$, $\rho_0/\rho_1 = 0.4$, $h_1/a = 0.5$
Solid 2	$k_{2_L} a = 30$, $k_{2_T} a = 70$, $\rho_0/\rho_2 = 0.3$

2.4. Results for a healthy fluid/solid/solid structure

The modulus of the complex component $T_{\alpha zz}$ ($\alpha = 0, 1, 2$) on the z-axis of the stress vector is shown via two cartographies (Figures 3), when an incident beam (adimensional frequency $k_0 a = 100$) interacts with the structure fluid 0/solid 1/solid 2. These stresses are normalized by the incident pressure P_{inc} at the centre of the emitter (note that the stress T_{0zz} in fluid 0 corresponds to the opposite of the pressure). The adimensional characteristics of each medium are given in Table I, and the structure is assumed to be healthy.

For both cartographies, the interferences in fluid 0 are due to the interaction of the incident field with the reflected field. On the other hand, the nodes and antinodes which can be observed at $\theta = 9°$ in Figure 3a) in solid 2 can be explained by the presence of both longitudinal and

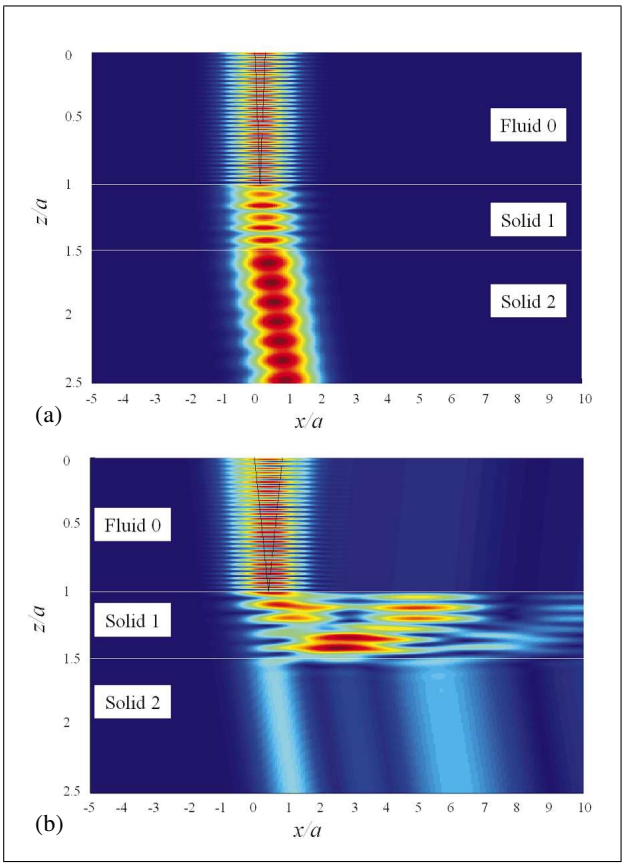

Figure 3. Cartographies of the modulus of the normalized stress $T_{\alpha zz}/P_{inc}$ ($\alpha = 0, 1, 2$) for a healthy structure fluid 0/solid 1/solid 2. The characteristics of each medium are given in Table I. a) $\theta = 9°$, b) $\theta = 23°$.

transversal waves which interact (the incidence is subcritical for these two types of waves). At an incidence $\theta = 23°$ slightly superior to the first critical angle for the interface fluid 0/solid 1 (Figure 3b), the successive reflections in layer 1 are highlighted by the presence of re- transmitted fields in fluid 0 and in solid 2. In particular, variations of amplitudes can be observed in solid 2 for the successive re-transmitted fields; these variations can be explained by constructive or destructive interferences between longitudinal and transversal waves in layer 1.

3. Kirchhoff approximation: Re-emission principle for the interaction of a plane wave with a finite size defect located on an interface

In section 4, the problem of the interaction between an incident bounded acoustic field and a plane interface with a finite defect will be solved, through the iterative procedure, using the re-emission principle, under Kirchhoff approximation.

The present section aims at explaining this principle when the simple case of a plane (monochromatic) incident wave is considered (the solution for an incident beam may then be deduced by superposition principle and Fourier integrals).

A plane wave, longitudinal or transversal, is assumed to propagate in solid 1 and to be incident on the interface (II), separating two elastic solids 1 and 2, both solids being considered as semi-infinite at this stage (Figure 1).

The interface (II) presents perfect bonding conditions (satisfying continuity conditions 10) everywhere except on the defect. The defect is described by other homogeneous boundary conditions, for example a complete debonding condition (see equation 11). As above-mentioned in section 2.2.2, "homogeneous" means that these conditions do not depend on the position all along the finite defect.

Since the exact analytical solution of the problem of interaction between an incident plane wave and an interface with a finite defect is not available, an approximate solution through Kirchhoff approximation is derived below.

Kirchhoff approximation may be well understood by using the concept that may be called the "re-emission principle" [38]. This principle is a consequence of the uniqueness of the solution for the problem of radiation in semi-infinite spaces.

Let us denote $\boldsymbol{u}_{1a}$ the incident (plane wave) field in solid 1, represented here by its displacement vector. The interaction of this field with interface (II), with the finite defect, yields a reflected field $\boldsymbol{u}_{1b}$ in solid 1 and a transmitted field $\boldsymbol{u}_{2a}$ in solid 2. As above-mentioned in section 2.2.1, the subscripts a and b mean that the field $\boldsymbol{u}_{1b}$ satisfies an appropriate radiation condition in solid 1 towards the negative values of z, whereas the field $\boldsymbol{u}_{2a}$ satisfies a radiation condition in solid 2 towards the positive values of z.

Of course, the exact expressions of the fields $\boldsymbol{u}_{1b}$ and $\boldsymbol{u}_{2a}$ are not known. But, for example, if the values of $\boldsymbol{u}_{1b}$ are known only on the interface (II), then, using these values as some emission data associated with the appropriate radiation condition in solid 1 towards $z < 0$, we would recover the solution $\boldsymbol{u}_{1b}$ in the whole semi-infinite space 1. This point results from the uniqueness of the solution of the radiation problem in a half-space when a convenient parameter describing the field (displacement, stress part...) is known on the limiting plane.

The same result holds for the determination of the field $\boldsymbol{u}_{2a}$ in the whole half-space 2 if its values are partially given on the interface (II).

Now, let us assume that the values of $\boldsymbol{u}_{1b}$ are known on the interface (II) only in an approximate way. Then, one may expect that solving the corresponding radiation problem in the half-space 1 will lead to an approximate solution of $\boldsymbol{u}_{1b}$ in the whole half-space.

The idea of Kirchhoff approximation is to obtain such approximate data on the interface (II) in the following way.

i) First we solve the interaction problem of the incident field $\boldsymbol{u}_{1a}$ with the interface (II) in the case of no defect, when the boundary conditions (10) are valid all along the interface. This problem will be solved easily for a plane

wave, which leads to an exact solution $\boldsymbol{u}_{1b}^{(h)}$ in the solid 1 (the superscript "h" stands for "healthy" interface).
ii) Secondly, we consider the same interaction problem for the interface (II) all along which we apply the boundary conditions (11) that are valid on the finite defect. Thus we consider the interface (II) as an "infinite" defect and we get the solution $\boldsymbol{u}_{1b}^{(i)}$ in the half-space 1 (the superscript "i" stands for "infinite defect" interface).
iii) We define the approximate data on the interface (II), leading to Kirchhoff approximation, by assigning to $\boldsymbol{u}_{1b}$ the values of $\boldsymbol{u}_{1b}^{(h)}$ outside of the defect, and the values of $\boldsymbol{u}_{1b}^{(i)}$ on the finite defect.

It appears at once that such an approximation consists in ignoring a part of the diffraction effects at the extremities of the finite defect, since the diffraction phenomenon alter, really speaking, the fields $\boldsymbol{u}_{1b}^{(h)}$ and $\boldsymbol{u}_{1b}^{(i)}$ in the neighborhood of the extremities of the defect.

With these Kirchhoff approximate data on the interface (II), the radiation problem in the half-space 1 may be solved by a plane wave decomposition, using spatial Fourier integrals, in the same way asthe incident beam has been computed (section 2.1).

However, this Fourier transforms method will be directly applicable, from a mathematical point of view, if we introduce an associated diffusion problem. The idea of the diffusion problem is to consider that the required approximate solution $\boldsymbol{u}_{1b}^{(k)}$, under Kirchhoff approximation, results from a modification of the solution $\boldsymbol{u}_{1b}^{(h)}$ for the healthy interface, due to the perturbation introduced by the finite defect. We then write this Kirchhoff solution in the form

$$\boldsymbol{u}_{1b}^{(k)} = \boldsymbol{u}_{1b}^{(h)} + \boldsymbol{u}_{1b}^{(s)}, \tag{22}$$

where the field $\boldsymbol{u}_{1b}^{(s)}$ is the part of the field that is scattered by the finite defect.

The scattered field $\boldsymbol{u}_{1b}^{(s)}$ is then obtained by solving the radiation problem in the half-space 1 with the following approximate data on the interface (II):

$$\boldsymbol{u}_{1b}^{(s)}(x, z = \zeta_2) = 0 \qquad \text{outside the defect,} \tag{23a}$$

$$\boldsymbol{u}_{1b}^{(s)}(x, z = \zeta_2) = \boldsymbol{u}_{1b}^{(i)}(x, z = \zeta_2) - \boldsymbol{u}_{1b}^{(h)}(x, z = \zeta_2) \qquad \text{on the defect.} \tag{23b}$$

The method to solve this radiation problem is identical to that used for a bounded emitter embedded in an infinite baffle, as it has been introduced in section 2.1 for the integral representation of the incident beam.

Similar procedure may be performed for the approximate solution $\boldsymbol{u}_{2a}^{(k)}$ in half-space 2, using the scattered field $\boldsymbol{u}_{2a}^{(s)}$.

In order to estimate the validity range of the Kirchhoff approximation, a comparison with the results obtained by the Geometrical Theory of Diffraction (GTD) [39, 40] (which is itself a high frequency approximation) has been performed in the case of the scattering of plane wave by a rectilinear slit in an infinite fluid medium. The results are in good agreement.

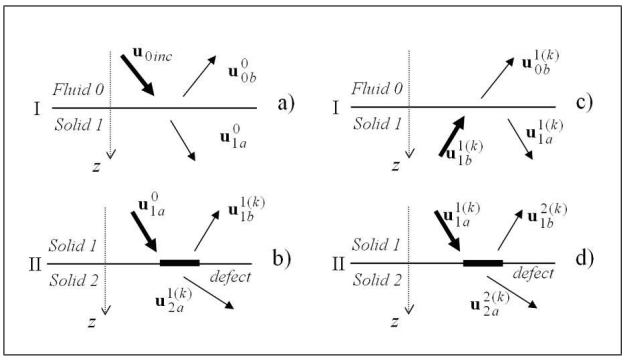

Figure 4. Successive steps of the iterative method. a) Step 0, b,c) step 1, d) beginning of the second step.

4. Interaction between a bounded beam and a plane layered structure with a finite defect on an internal interface: Iterative Kirchhoff approximation method

This section aims at explaining the implementation of Kirchhoff approximation method in the case of the interaction of a bounded beam with the structure fluid 0/solid 1/solid 2 which includes a finite-size defect located on interface II. In this problem, two different effects have to be taken into account: i) the diffraction of a field on a defect located on an interface using Kirchhoff approximation, ii) the transmission of a field through all the other healthy interfaces of the structure. Under this approximation, the method used here consists in considering separately effects i) and ii), though the problem could be solved globally, and then in implementing an iterative method, which is presented in this section.

The implementation of this iterative method using displacement fields is first given in section 4.1 and some results are presented in section 4.2.

4.1. Implementation of the iterative method

The consecutive steps of the iterative method are numbered from (0) to (n), step (0) corresponding to the transmission through the first interface for the first time, and subsequent numbers (p) corresponding to the interaction with the defect for the p-th time.

The principle of the iterative method is applied to monochromatic fields of displacements, decomposed into plane waves (see section 2).

It is worth noting that, in order to be more concise, we chose in this paper, to explicit only the reflection problem in fluid 0, but similar expressions can be easily obtained for the transmission problem in solid 2.

4.1.1. Step (0)

The incident field $\boldsymbol{u}_{0,inc}$ is first decomposed into plane waves using the procedure described in section 2.1 (see also Figure 4a). The transmitted field $\boldsymbol{u}_{1a}^{0}$ in solid 1 and

the reflected field $\boldsymbol{u}_{0b}^0$ can then be obtained (with notations analogous to those used in equations 18 and 19):

$$\boldsymbol{u}_{1a}^0(x,z) = \sum_{\eta=L,T} \int_{-\infty}^{+\infty} A_{1_\eta}^0(k_{x_e}) \boldsymbol{P}_{1a_\eta} \cdot \exp\left\{ \mathrm{i}\left[k_x x + k_{1z_\eta}\left(z-\zeta_1\right)\right]\right\} \mathrm{d}k_{x_e}, \tag{24}$$

and

$$\boldsymbol{u}_{0b}^0(x,z) = \int_{-\infty}^{+\infty} B_0^0(k_{x_e}) \boldsymbol{P}_{0b} \cdot \exp\left\{ \mathrm{i}\left[k_x x - k_{0z}\left(z-\zeta_1\right)\right]\right\} \mathrm{d}k_{x_e}, \tag{25}$$

where the displacement amplitudes of the longitudinal and transversal plane waves constituting the transmitted field $\boldsymbol{u}_{1a}^0$ are denoted respectively A_{1L}^0 and A_{1T}^0, and where the displacement amplitude in fluid 0 is denoted B_0^0. Note that these amplitudes are deduced from the solving of a linear system of three equations.

4.1.2. Step (1)

The following step (step 1) consists in studying the interaction of the field $\boldsymbol{u}_{1a}^0$ with the interface II on which the defect is located, considering again the two solid media 1 and 2 as both semi-infinite (see Figure 4b).

Solving the problem of the interaction of the transmitted field $\boldsymbol{u}_{1a}^0$ with a finite-size defect located on the interface II, using Kirchhoff approximation, needs to solve two preliminary problems of the interaction between the incident beam and the structure; the first one with the healthy interface (problem (h)), the second one with an infinite interface yielding the defect behavior (infinite defect, problem (i)). These problems are solved separately for each plane wave of amplitude $A_{1_\eta}^0(k_{x_e})$ with $\eta = L, T$, which generates waves of amplitudes $B_{1_\eta}^{1(*)}(k_{x_e})$ propagating in solid 1 towards $z < 0$ and waves of amplitudes $A_{2_\eta}^{1(*)}(k_{x_e})$ propagating in solid 2 towards $z > 0$, with $\eta = L, T$ and $(*) = (h), (i)$.

Similarly to what has been done in section 3 (see equation 22), the scattered field $\boldsymbol{u}_{1b}^{1(s)}$ can be introduced for the reflection problem, and its approximated values can be calculated on interface II at $z = \zeta_2$. It should be noticed that here, contrary to section 3, the calculation is not performed for each plane wave, but straightforwardly for bounded beams, in order to minimize computation time.

In other words, similarly to equations (23), the reemission data can be written as

$$\boldsymbol{u}_{1b}^{1(s)}(x, z=\zeta_2) = 0 \qquad \text{outside the defect,} \tag{26a}$$

$$\boldsymbol{u}_{1b}^{1(s)}(x, z=\zeta_2) = \boldsymbol{u}_{1b}^{1(i)}(x, z=\zeta_2) - \boldsymbol{u}_{1b}^{1(h)}(x, z=\zeta_2) \qquad \text{on the defect,} \tag{26b}$$

where, using the notations of equation (19),

$$\boldsymbol{u}_{1b}^{1(*)}(x, z=\zeta_2) = \sum_{\eta=L,T} \int_{-\infty}^{+\infty} B_{1_\eta}^{1(*)}(k_{x_e}) \boldsymbol{P}_{1b_\eta} \cdot \exp\left(\mathrm{i}k_x x\right) \mathrm{d}k_{x_e}, \quad (*) = (h), (i). \tag{27}$$

It should be noted that it is useless to calculate integrals (27) for abscissa x which do not belong to the definition domain of the defect, since the scattered field is zero outside the defect (see equation 26a).

Once the reemission data $\boldsymbol{u}_{1b}^{1(s)}(x, z = \zeta_2)$ are calculated on the defect, the latter behaves like a passive emitter in a baffle and thus, the scattering problem may be solved by a method similar to the decomposition of the incident beam using Fourier integrals (see section 2.1). As this decomposition is done here in an isotropic solid medium, each plane wave can be either longitudinal or transversal, their corresponding displacement amplitudes being denoted respectively $B_{1L}^{1(s)}$ and $B_{1T}^{1(s)}$ for the propagation in solid 1. It should be noted that, due to the fact that the re-emission data are given on interface II, which is parallel to x-axis, the plane wave decomposition is performed through a Fourier Transform with respect to the x variable, so that the obtained amplitudes depends directly on k_x (and no longer on k_{x_e}). Therefore, the subsequent integrations will be done using k_x (instead of k_{x_e}).

In other words, the propagation in solid 1 of the reemitted field can be written as (with notations analogous to those used in equation 19):

$$\boldsymbol{u}_{1b}^{1(s)}(x,z) = \sum_{\eta=L,T} \int_{-\infty}^{+\infty} B_{1_\eta}^{1(s)} \boldsymbol{P}_{1b_\eta} \cdot \exp\left[-\mathrm{i}k_{1z_\eta}\left(z-\zeta_2\right)\right] \exp\left(\mathrm{i}k_x x\right) \mathrm{d}k_x, \tag{28}$$

which permits to deduce the amplitudes $B_{1_\eta}^{1(s)}(k_x)$, similarly to equation (5), through the inverse Fourier transform system

$$\sum_{\eta=L,T} B_{1_\eta}^{1(s)}(k_x) \boldsymbol{P}_{1b_\eta} = \frac{1}{2\pi} \int_{-\infty}^{+\infty} \boldsymbol{u}_{1b}^{1(s)}(x, z=\zeta_2) \exp\left(-\mathrm{i}k_x x\right) \mathrm{d}x, \tag{29}$$

where this integral has its integration domain limited to the defect, since the data are zero outside (equation 26). Equation (29) is a linear system of two equations (coming from their projections on x- and z-axis) with the two unknowns $B_{1_\eta}^{1(s)}$, $\eta = L, T$.

A similar reasoning leads to the scattered field $\boldsymbol{u}_{2a}^{1(s)}$ and to expression of amplitudes $A_{2_\eta}^{1(s)}$, $\eta = L - T$, in solid 2.

At this stage, the scattered field $\boldsymbol{u}_{1b}^{1(s)}$ is known in layer 1. Thus, the total interaction term $\boldsymbol{u}_{1b}^{1(k)}$ in layer 1 for step 1, under Kirchhoff approximation, can be written, for this step 1, as the summation of the scattered field $\boldsymbol{u}_{1b}^{1(s)}$ and of the field $\boldsymbol{u}_{1b}^{1(h)}$ in the healthy structure (see equation 22):

$$\boldsymbol{u}_{1b}^{1(k)} = \boldsymbol{u}_{1b}^{1(h)} + \boldsymbol{u}_{1b}^{1(s)}. \tag{30}$$

However, it should be noted that the Fourier integrals (27) and (28) which express each term of the right hand side of equation (30) are calculated using different integration variables: k_{x_e} for $\boldsymbol{u}_{1b}^{1(h)}$ and k_x for $\boldsymbol{u}_{1b}^{1(s)}$.

These Fourier transforms are now used in order to calculate the interaction of each field with interface I. Each scattered plane wave with amplitude $B_{1_\eta}^{1(s)}(k_x)$ propagating in solid 1 towards $z < 0$ is now an incident wave for interface I between fluid 0 and solid 1, which generates "transmitted" waves with amplitudes $B_0^{1(s)}(k_x)$ in fluid 0 and "reflected" waves with amplitudes $A_{1_\eta}^{1(s)}(k_x)$ in solid 1 (see Figure 4c). These amplitudes are deduced from the three classical boundary conditions for plane waves at $z = \zeta_1$. The same reasoning can be done for each "incident" plane wave with amplitudes $B_{1_\eta}^{1(h)}(k_{x_e})$ coming from the problem for a healthy interface II, which generates waves of amplitudes $B_0^{1(h)}(k_{x_e})$ in fluid 0 and $A_{1_\eta}^{1(h)}(k_{x_e})$ in solid 1.

4.1.3. Step (2) and following steps

The field $\boldsymbol{u}_{1a}^{1(k)}$ can now be considered as an incident field for interface II with the defect (see Figure 4d).

In the same way as for the calculation in the step 0 of the wave amplitude $A_{1_\eta}^{0}(k_{x_e})$, each plane wave with amplitudes $A_{1_\eta}^{1(s)}(k_x)$ and $A_{1_\eta}^{1(h)}(k_{x_e})$ interacts with interface II including the finite-size defect. In the same manner as in step 1 (see section 4.1.2), two preliminary problems have to be solved in order to obtain the re-emission data on interface II: the problem (h) for a healthy interface II and the problem (i) with an infinite defect on interface II.

- The amplitudes of the waves generated by the problem (h) (resp. (i)), when the scattered field with amplitudes $A_{1_\eta}^{1(s)}(k_x)$ is the incident field on interface II, are respectively denoted $B_{1_\eta}^{2(h)(s)}(k_x)$ and $B_{1_\eta}^{2(i)(s)}(k_x)$, where the superscript "2" stands for "second step".
- The amplitudes of the waves generated by the problem (h) (resp. (i)), when the "healthy" field with amplitudes $A_{1_\eta}^{1(h)}(k_{x_e})$ is the incident field on interface II, are respectively denoted $B_{1_\eta}^{2(h)(h)}(k_{x_e})$ and $B_{1_\eta}^{2(i)(h)}(k_{x_e})$, where the superscript "2" stands for "second step". It should be noted that, here, these amplitudes depend on k_{x_e}.

Similarly to equations (26), but here for the second step, the reemission data can be written as

$$\boldsymbol{u}_{1b}^{2(s)}(x, z = \zeta_2) = 0 \qquad \text{outside the defect,} \tag{31a}$$

$$\boldsymbol{u}_{1b}^{2(s)}(x, z = \zeta_2) = \boldsymbol{u}_{1b}^{2(i)}(x, z = \zeta_2) - \boldsymbol{u}_{1b}^{2(h)}(x, z = \zeta_2) \qquad \text{on the defect,} \tag{31b}$$

where

$$\boldsymbol{u}_{1b}^{2(*)}(x, z = \zeta_2) = \boldsymbol{u}_{1b}^{2(*)(s)}(x, z = \zeta_2) + \boldsymbol{u}_{1b}^{2(*)(h)}(x, z = \zeta_2), \quad (*) = (h), (i), \tag{32}$$

and where, using the notations of equation (27),

$$\boldsymbol{u}_{1b}^{2(*)(h)}(x, z = \zeta_2) = \sum_{\eta=L,T} \int_{-\infty}^{+\infty} B_{1_\eta}^{2(*)(h)}(k_{x_e}) \boldsymbol{P}_{1b_\eta} \cdot \exp\left(\mathrm{i}k_x x\right) \mathrm{d}k_{x_e}, \quad (*) = (h), (i), \tag{33}$$

and

$$\boldsymbol{u}_{1b}^{2(*)(s)}(x, z = \zeta_2) = \sum_{\eta=L,T} \int_{-\infty}^{+\infty} B_{1_\eta}^{2(*)(s)}(k_{x_e}) \boldsymbol{P}_{1b_\eta} \cdot \exp\left(\mathrm{i}k_x x\right) \mathrm{d}k_{x_e}, \quad (*) = (h), (i). \tag{34}$$

Now, the re-emission data are calculated, and the scattered field $\boldsymbol{u}_{1b}^{2(s)}$ can be calculated in the same manner as in the previous step, using the decomposition into plane waves, which permits to calculate the interaction with interface I. A similar reasoning leads to the scattered field $\boldsymbol{u}_{2a}^{2(s)}$ in solid 2. This ends step 2.

The calculation process for the next steps follows exactly the same scheme as for the step 2.

It may be noted that in order to avoid, at each step, the coexistence of amplitudes which depend on k_x and on k_{x_e}, a Fourier transform on the interface II, from the variable x to a new variable k_x may be performed for the healthy structure solution, since for a bounded beam, the values of the field on the interface, as a function of x, admit a Fourier Transform. However, this simplifying procedure introduces some numerical error and it is preferable to apply it only after some steps of the iterative process. In the results presented in section 4.2, it has been applied at the second step only (see equation 40).

4.1.4. End of the iterative process and final result

The upper order iteration corresponds to the n-th approximate re-emitted field $\boldsymbol{u}_{0b}^{n(k)}$, considering its pressure field $P_{0b}^{n(k)}$ in the fluid 0, which gets out the physical (x, z) domain numerically defined by the user, or it is given by the condition which expresses that the quadratic mean value of this pressure becomes less than a small value ε such that

$$\frac{1}{N\sqrt{P_{inc}\bar{P}_{inc}}} \sum_{r=1}^{N} \sqrt{P_{0b}^{n(k)}(x_r, \zeta)\bar{P}_{0b}^{n(k)}(x_r, \zeta)} < \varepsilon, \tag{35}$$

where P_{inc} is the incident pressure at the centre of the emitter (in order to normalize the pressure $P_{0b}^{n(k)}$), N is the number of samples for describing the variable x, x_r is the r-th sample for x, $\bar{X}$ is the complex conjugate of X, with $\zeta = 0.75a$ (see Figure 1), ε being usually taken equal to 10^{-4}. The number n of iterations clearly depends on the incident angle of the acoustic beam and on the location of the defect.

The final approximated reflected field in fluid 0 under Kirchhoff approximation is then given by

$$\boldsymbol{u}_{0b}^{(k)} = \boldsymbol{u}_{0b}^{0} + \sum_{p=1}^{n} \boldsymbol{u}_{0b}^{p(k)}, \tag{36}$$

with

$$\boldsymbol{u}_{0b}^{p(k)} = \boldsymbol{u}_{0b}^{p(h)} + \boldsymbol{u}_{0b}^{p(s)}, \quad p = 1, \ldots, n, \tag{37}$$

which yields

$$\boldsymbol{u}_{0b}^{(k)} = \boldsymbol{u}_{0b}^{0} + \sum_{p=1}^{n} \boldsymbol{u}_{0b}^{p(h)} + \sum_{p=1}^{n} \boldsymbol{u}_{0b}^{p(s)}, \tag{38}$$

i.e.

$$\boldsymbol{u}_{0b}^{(k)} = \boldsymbol{u}_{0b}^{(h)} + \boldsymbol{u}_{0b}^{(s)}. \tag{39}$$

It should be noted that the field $\boldsymbol{u}_{0b}^{(s)}$, which represents here the sum of all the partial scattered fields at each step, may be different from the scattered field which could be obtained straightforwardly by a global method (see [38]). In this latter method, parasite echoes could be produced on the defect.

The reflected pressure fields $P_{0b}^{(*)}$ in fluid 0, corresponding to the problems for a healthy interface II [$(*) = (h)$], or for a defect on interface II either of infinite extent [$(*) = (i)$], or of finite extent [$(*) = (k)$] under Kirchhoff approximation, are then given by

$$P_{0b}^{(*)}(x,z) = -\mathrm{i}\rho_0\omega V_0 \int_{-\infty}^{+\infty} B_0^{(*)}(k_{x_e}) \cdot \exp\left[-\mathrm{i}k_0 z\left(z-\zeta_1\right)\right] \exp\left(\mathrm{i}k_x x\right) \mathrm{d}k_{x_e}, \quad (*) = (h), (i), \tag{40a}$$

$$\begin{aligned} P_{0b}^{(k)}(x,z) = -\mathrm{i}\rho_0\omega V_0 \cdot \Bigg\{ & \int_{-\infty}^{+\infty} B_0^{0}(k_{x_e}) \exp\left[-\mathrm{i}k_{0z}\left(z-\zeta_1\right)\right] \exp\left(\mathrm{i}k_x x\right) \mathrm{d}k_{x_e} \\ & + \int_{-\infty}^{+\infty} B_0^{1(h)}(k_{x_e}) \exp\left[-\mathrm{i}k_{0z}\left(z-\zeta_1\right)\right] \exp\left(\mathrm{i}k_x x\right) \mathrm{d}k_{x_e} \\ & + \int_{-\infty}^{+\infty} B_0^{1(s)}(k_{x_e}) \exp\left[-\mathrm{i}k_{0z}\left(z-\zeta_1\right)\right] \exp\left(\mathrm{i}k_x x\right) \mathrm{d}k_{x} \\ & + \int_{-\infty}^{+\infty} \sum_{p=2}^{N} B_0^{p(k)}(k_x) \exp\left[-\mathrm{i}k_{0z}\left(z-\zeta_1\right)\right] \cdot \exp\left(\mathrm{i}k_x x\right) \mathrm{d}k_x \Bigg\}, \end{aligned} \tag{40b}$$

with, similar to equation (37),

$$B_0^{p(k)} = B_0^{p(h)} + B_0^{p(s)}, \quad p = 2, \ldots, n. \tag{40c}$$

Note that k_x is the integration variable in the last two integrals of equation (40b), whereas it is understood as a function of the integration variable k_{x_e} in the first two ones.

4.2. Results and comparisons between healthy and non-healthy fluid/solid/solid structures

This section aims at providing some results for the same structure as that studied in section 2.4 (Figure 3), but including here a finite-size defect of length $2L$ (full delaminating), located on the interface II defined by d (see Figure 1). The adimensional characteristics of each medium are given in Table I.

The cartographies present, like in section 2.4, the modulus of the normalized complex z-component $T_{\alpha zz}/P_{inc}$ ($\alpha = 0, 1, 2$) of the stress vector when an incident beam (adimensional frequency $k_0 a = 100$) interacts with the structure fluid 0/solid 1/solid 2. The cuts in fluid 0 show the normalized reflected pressure moduli $|P_{0b}^{(*)}|/P_{inc}$ (given by equation 40) in a plane parallel to the interfaces

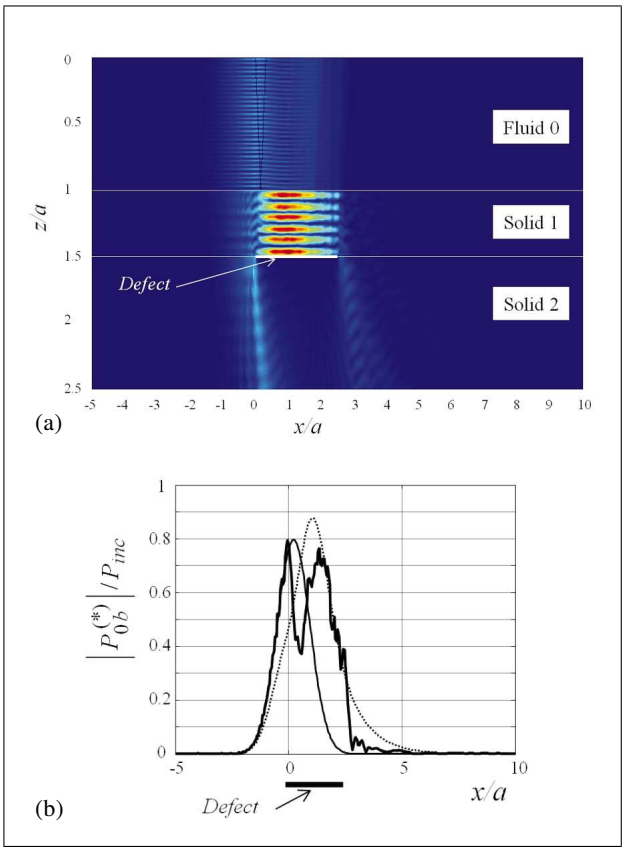

Figure 5. Incident beam such that $\theta = 9°$. a) Cartography of the modulus of the normalized stress $T_{\alpha zz}/P_{inc}$ ($\alpha = 0, 1, 2$) for a structure with a defect such that $2L/a = 9$ and $d/a = 1.25$. b) Modulus of the normalized reflected pressure $|P_{0b}^{(*)}|/P_{inc}$ in fluid 0, for a cut at $\zeta/a = 0.75$. Thin solid line $(*) = (h)$, dotted line $(*) = (i)$ and thick solid line $(*) = (k)$.

($\zeta/a = 0.75$) as a function of x/a (see Figure 1): thin solid line for an healthy interface II $(*) = (h)$, dotted line for an infinite defect $(*) = (i)$ on interface II, and thick solid line for a finite size defect $(*) = (k)$ on interface II.

4.2.1. Influence of the incidence and of the length of the defect

The comparison between the cartography which corresponds to a finite-size defect on interface II and $\theta = 9°$ (Figure 5a) and the cartography which corresponds to the healthy structure in the same conditions (Figure 3a) show that the transmission through the interface II by the field is strongly modified by to the presence of the defect, which causes more reflections in layer 1, and that a shadow region behind the defect is observed in solid 2. Moreover, for a finite-length defect, diffraction effects appear on the reflected pressure $P_{0b}^{(k)}$ (thick solid curve on Figure 5b). As expected, this curve is closed to the thin solid curve corresponding to the reflected pressure $P_{0b}^{(h)}$ as long as the beam does not encounter the defect, and follows the dotted curve corresponding to the reflected pressure $P_{0b}^{(i)}$ when the beam encounters the defect. The differences between the fields are significant enough to allow a good detection of the defect.

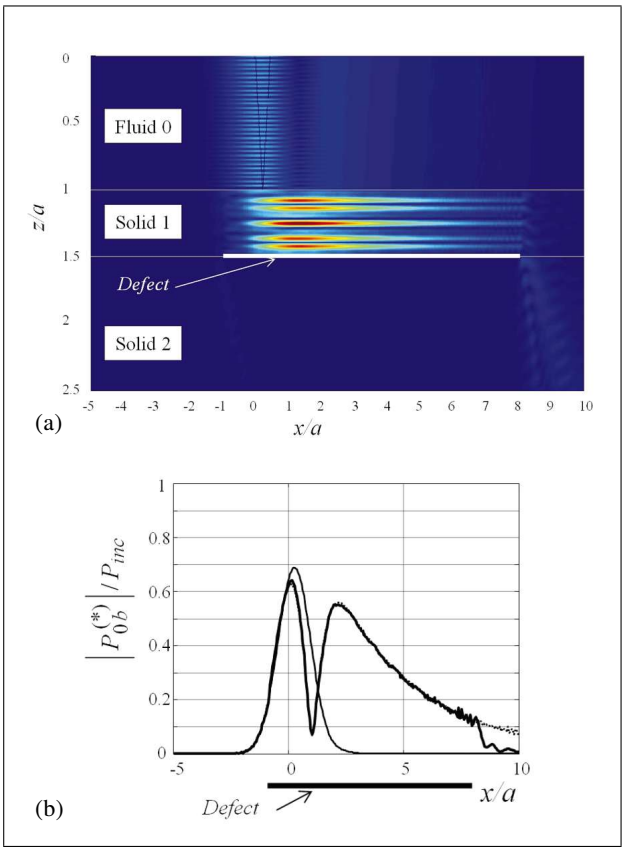

Figure 6. Incident beam such that $\theta = 12.82°$. a) Cartography of the modulus of the normalized stress $T_{\alpha zz}/P_{inc}$ ($\alpha = 0, 1, 2$) for a structure with a defect such that $2L/a = 9$ and $d/a = 3.5$. b) Modulus of the normalized reflected pressure $|P_{0b}^{(*)}|/P_{inc}$ in fluid 0, for a cut at $\zeta/a = 0.75$. Thin solid line $(*) = (h)$, dotted line $(*) = (i)$ and thick solid line $(*) = (k)$.

If a Lamb mode can propagate in the structure with an infinite defect on interface II, and if the length of the defect is long enough, it is also possible to create a Lamb mode between interface I and the defect (Figures 6, $\theta = 12.82°$). The propagation of a symmetric Lamb mode in the layer 1 and its re-radiation in fluid 0 can be observed on Figure 7a). Due to the length of the defect ($2L = 9a$), the curves corresponding to the reflected pressures $P_{0b}^{(k)}$ and $P_{0b}^{(i)}$ (Figure 6b) are very close, except at the end of the defect, where diffraction effects on the right edge of the defect appear. The strong trough in the pressure profile is a classical feature when a Rayleigh wave or a Lamb wave is generated.

4.2.2. Convergence rate of the iterative process

This section aims at providing some explanations on the convergence rate of the iterative method, complementary to those already given in section 4.1.4. As explained in that section, the successive iterations take place until the n-th approximate re-emitted displacement field $\boldsymbol{u}_{0b}^{n(k)}$ in the fluid 0 or the associated pressure gets out of the physical (x, z) domain numerically defined by the user, or when the n-th re-emitted quadratic mean value of the pressure field becomes less than a small value ε (see equation 35).

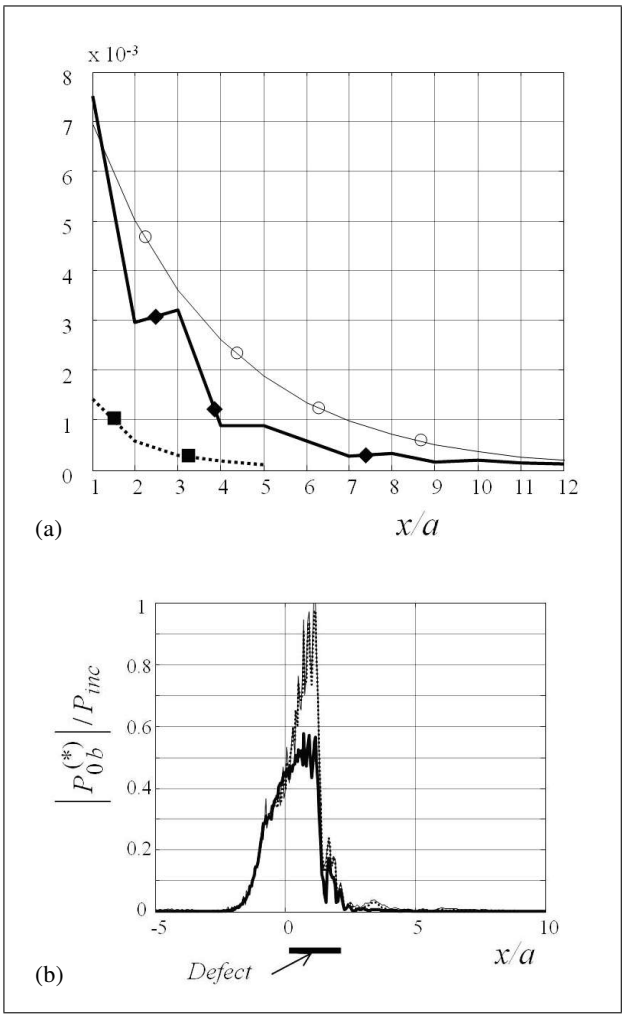

Figure 7. Convergence of the iterative method, $L = a$. a) Quadratic mean given by equation (26) as a function of the number n of iterations. Thin solid line with open circles $\theta = 0°$, $d = 0$. Thick solid line with closed diamonds $\theta = 9°$, $d/a = 0.1584$. Dotted line with closed squares $\theta = 11°$, $d/a = 0.1$. b) Modulus of the normalized reflected pressure $|P_{0b}^{(k)}|/P_{inc}$ under Kirchhoff approximation in fluid 0, for a cut at $\zeta/a = 0.75$, when $\theta = 9°$. Thin solid line: 13 iterations, dotted line: 4 iterations, thick solid line: 2 iterations.

Figure 7a shows the quadratic mean value of the pressure given by the left hand side of equation (35) as a function of the number of iterations, for the same structure, but with three different incident angles: thin solid line with open circles for $\theta = 0°$, thick solid line with closed diamonds for $\theta = 9°$, and dotted line with closed squares for $\theta = 11°$. The locations of the defect have been chosen in each case such that the point O corresponding to the impact of the incident beam axis on interface I (see Figure 1) be located at the same abscissa than the centre of the defect. It can be observed on Figure 7a that the convergence of the iterative process is faster when $\theta = 11°$ and $\theta = 9°$ than when $\theta = 0°$ because, for normal incidence, the acoustic field oscillates between interfaces I and II, and the loss of energy is only due to the successive reflections on these interfaces. On the contrary, at incidences $\theta = 9°$ and $\theta = 11°$,

there are of course successive reflections, but these reflections gradually shift the dominant values of the field outside of the computation window in the physical space. This means that, for normal incidence, the convergence rate is only due to the convergence rate of the geometric series (see the beginning of section 2.2.2.), and for a non-normal incidence, the convergence rate may result from the fact that the field get out the computation window. Moreover, it can be observed that the thick solid line corresponding to $\theta = 9°$ presents an increase for the third iteration: this is due to the fact that, at this step, the beam interacts completely with the defect, whereas at former steps, a part of the beam did not encounter the defect.

Figure 7b presents the reflected fields $P_{0b}^{(k)}$ in fluid 0 for 2, 4 and 13 iterations, when $\theta = 9°$, showing that the convergence is nearly reached after 4 iterations.

4.2.3. Influence of the location of the defect

Results presented on Figures 8 correspond to the same configuration as that of Figure 5, except that the location of the defect is translated along the interface II: $d/a = 1.25$ for Figure 5, $d/a = 0.75$ for Figure 8a, $d/a = 1.75$ for Figure 8b, and $d/a = 2.75$ for Figure 8c (see Figure 1 for the geometry and the definition of d).

When $d/a = 2.75$ (Figure 8c), the effect of the defect, slightly visible, is only due to the diffraction coming from the left edge of the defect. When $d/a = 0.75$ (Figure 8a), the defect is clearly visible, the main part of the reflected field $P_{0b}^{(k)}$ (thick solid line) is close to the field $P_{0b}^{(i)}$ (dotted line), and the effects of the diffraction on both edges of the defect appear clearly. When $d/a = 1.75$ (Figure 8b), the amplitude of the reflected field $P_{0b}^{(k)}$ (thick solid line) coincides partially with the amplitude of the field $P_{0b}^{(h)}$ (thin solid line) for the healthy structure, except where effects of diffraction on the left edge of the defect appear (the diffraction field coming from the right edge is slightly visible).

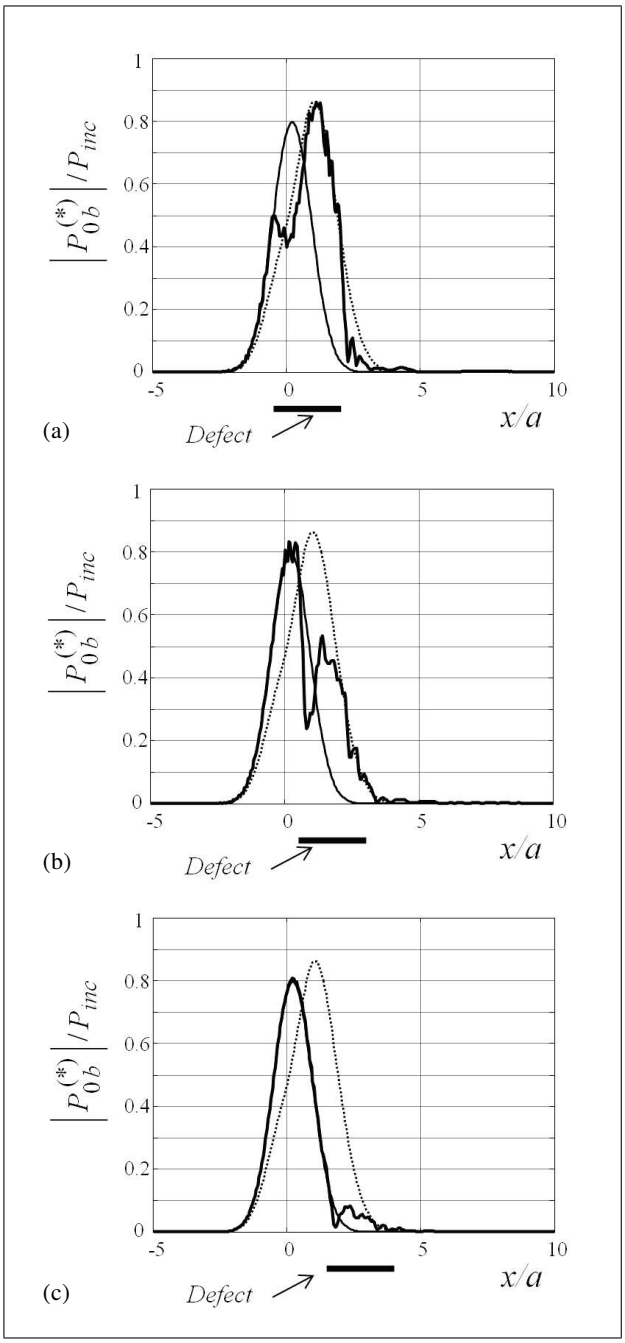

Figure 8. Modulus of the normalized reflected pressure $|P_{0b}^{(*)}| / P_{inc}$ in fluid 0. Thin solid line $(*) = (h)$, dotted line $(*) = (i)$ and thick solid line $(*) = (k)$. $\theta = 9°$, $\zeta/a = 0.75$, $2L/a = 2.5$. a) $d/a = 0.75$, b) $d/a = 1.75$, c) $d/a = 2.75$.

5. Conclusions

An iterative method, based upon both the decomposition of the fields into plane waves and a "passive re-emission" method under Kirchhoff approximation, has been developed in order to solve the problem of interaction between an ultrasonic bounded beam, emitted by a plane transducer, and a defect located on the plane interface between the two solids of a fluid / solid / solid structure.

A comparison between the results provided by this method and by the Geometrical Theory of Diffraction (both adequate in the high frequency range) for a defect located in a fluid, shows a good agreement in a large frequency range and for every incident angles of interest, to estimate the validity of this new method.

The main advantage of the method is to reduce drastically the time needed to provide cartographies of the acoustic fields in the physical space (less than one minute on a usual personal computer), which would be of interest when treating complex situations as those usually computed using finite element methods (current packages).

This improvement results mainly from using simple classical trapezoid method associated to a matrix formalism to calculate the spatial Fourier integrals, which avoids constraints between the set of integration variables (wave number components) and the spatial variables chosen for the representation area in the physical space. It is then possible to very easily obtain acoustic field cartographies or

cuts of the pressure in the external fluid along a plane parallel to the interfaces, showing more particularly the effects of the influence of the defect on the propagation of the ultrasonic beam in the structure (in comparison with the case of the healthy structure).

The iterative process used stops when the quadratic mean value of the re-emitted pressure, for the running step, is less than a prescribed small value. It has been shown that the convergence rate of the method depends on the incident angle of the beam: the convergence is slower for normal or quasi-normal incidences. So, in this case, it may be preferable to use a direct method for the computation of the fields [38]. In contrast, the convergence may be faster when the incident angle reaches any non vanishing values, since after several iterations, the predominant values of the pressure field are found outside of the representation area, due to the successive reflections on the interfaces an on the defect. It has been shown that in this case, the iterative method is better adapted than a direct method.

A number of geometrical configurations have been studied. For rather long defects (delaminations), a Lamb wave may be generated between the defect and the upper interface. The location of the defect with respect to the impact zone of the beam has a great influence on the pressure pattern in the fluid. If the defect is near the impact zone, the pressure field may be quite the same as for a structure with an infinite delamination in the case of a narrow beam. On the contrary, when the defect is far from the impact zone, in the "downstream" direction, a number of successive reflections may be necessary to reach the defect in this situation, a direct method would give a wrong result. Between these two extreme cases, the pressure field values alternate between those obtained for the structure with an infinite delamination and those obtained for the healthy structure, with transition zones yielding diffraction effects on the edges of the defect.

References

[1] J. D. Achenbach: Modeling for quantitative non-destructive evaluation. Ultrasonics **40** (2002) 1–10.

[2] D. A. Mendelsohn, J. D. Achenbach, L. M. Keer: Scattering of elastic waves by a surface-breaking crack. Wave Motion **2** (1980) 277–292.

[3] R. J. Brind, J. D. Achenbach: Scattering of longitudinal and transverse waves by a sub-surface crack. J. Sound. Vib. **78** (1981) 555–563.

[4] T. Kundu, A. K. Mal: Diffraction of elastic waves by a surface crack on a plate. J. Appl. Mech. **48** (1981) 570–576.

[5] Y. C. Angel: Scattering of Love waves by a surface-breaking crack. J. Appl. Mech. **53** (1986) 587–592.

[6] W. Hassan, W. Veronesi: Finite element analysis of Rayleigh wave interaction with finite-size, surface-breaking cracks. Ultrasonics **41** (2003) 41–52.

[7] B. Masserey, E. Mazza: Analysis of the near-field ultrasonic scattering at a surface crack. J. Acoust. Soc. Am. **118** (2005) 3585–3594.

[8] A. Boström: Elastic wave scattering from an interface crack: Antiplane strain. J. Appl. Mech. **54** (1987) 503–508.

[9] Y. Chevalier, M. Louzar, G. A. Maugin: Influence of interfacial slits with elastic slip on the propagation of SH waves. J. Acoust. Soc. Am. **98** (1995) 445–453.

[10] Y. S. Wang, D. Gross: Transfer matrix method of wave propagation in a layered medium with multiple interface cracks: Antiplane case. J. Appl. Mech. **68** (2001) 499–503.

[11] J. Qu: Interface crack loaded by a time-harmonic plane wave. Int. J. Solid Struct. **31** (1994) 329–345.

[12] K. N. Srivastava, R. M. Palaiya, O. P. Gupta: Interaction of longitudinal wave with a penny-shaped crack at the interface of two bonded dissimilar elastic solids - II. Int. J. Fracture **15** (1979) 591–599.

[13] A. Boström, L. Peterson: Scattering of acoustic waves by a circular disc in the interface between two fluids. J. Acoust. Soc. Am. **90** (1991) 3338–3343.

[14] A. Boström: Acoustic scattering by sound-hard rectangle. J. Acoust. Soc. Am. **90** (1991) 3344–3347.

[15] A. Baltazar, S. I. Rokhlin, C. Pecorari: On the relationship between ultrasonic and micro-structural properties of imperfect interfaces in layered solids. – In: Review of Progress in QNDE. D. O. Thomson, D. E. Chimenti (eds.). Plenum, New York, 1999, 18B, 1463–1470.

[16] A. Baltazar, S. I. Rokhlin, C. Pecorari: On the relationship between ultrasonic and micromechanical properties of contacting rough surfaces. J. Mech. Phys. Solids **50** (2002) 1397–1416.

[17] A. Baltazar, L. Wang, B. Xie, S. I. Rokhlin: Inverse ultrasonic determination of imperfect interfaces and bulk properties of a layer between two solids. J. Acoust. Soc. Am. **114** (2003) 1424–1433.

[18] S. I. Rokhlin, L. Wang, B. Xie, V. A. Yakovlev, L. Adler: Modulated angle beam ultrasonic spectroscopy for evaluation of imperfect interfaces and adhesive bonds. Ultrasonics **42** (2004) 1037–1047.

[19] G. Shkerdin, C. Glorieux: Interaction of Lamb modes with delaminations in plates coated by highly absorbing materials. IEEE Trans. Ultrason. Ferroelec. Freq. Control. **54** (2007) 368–377.

[20] J. W. Goodman: Introduction to Fourier optics. MacGraw Hill, New York, 1981.

[21] B. Hosten, M. Deschamps: Transmission ultrasonore en faisceau borné d'une interface plane à l'aide du spectre angulaire d'ondes planes. Traitement du Signal **2** (1985) 195–199.

[22] M. E. Schaffer, P. A. Lewin, J. M. Reid: Propagation through inhomogeneous media using the angular spectrum method. Proc. IEEE Trans. Ultrason. Symp. **2** (1987) 943–945.

[23] M. E. Schaffer, P. A. Lewin: Transducer characterization using the angular spectrum method. J. Acoust. Soc. Am. **85** (1989) 2204–2214.

[24] A. Souissi: Développement des méthodes numériques et expérimentales pour l'étude du champ acoustique de transducteurs ultrasonores en présence d'une interface fluide-solide (réflexion-transmission). PhD thesis, Université de Technologie de Compiègne, 1987.

[25] J. F. de Belleval, A. Souissi, P. Gatignol, N. Mercier: Modélisation numérique du champ acoustique de transducteurs en présence d'interfaces quelconques ou de milieux multicouches. Proc. IXème JESPA, Marseille-France, 1990.

[26] D. Orofino, P. Pedersen: Angle-dependent spectral distortion for an infinite planar fluid-fluid interface. J. Acoust. Soc. Am. **92** (1992) 2883–2889.

[27] D. Orofino, P. Pedersen: An angular spectrum technique for calculating receiver output signals for pulse-echo ultra-

sound insonification of elastics plates. Proc. IEEE. Ultrason. Symp. **1** (1992) 667–670.

[28] D. Orofino, P. Pedersen: Efficient angular spectrum decomposition of acoustic source. Part I: Theory. IEEE Trans. Ultrason. Ferroelec. Freq. Control. **40** (1993) 238–249.

[29] D. Orofino, P. Pedersen: Efficient angular spectrum decomposition of acoustic sources. Part II: Results. IEEE Trans. Ultrason. Ferroelec. Freq. Control. **40** (1993) 250–257.

[30] D. Orofino, P. Pedersen: Evaluation of IP-ASD for elastic media via angular spectrum decomposition. J. Acoust. Soc. Am. **93** (1993) 1235–1248.

[31] P. Pedersen, D. Orofino: Modeling of received ultrasound signals from finite planar targets. IEEE Trans. Ultrason. Ferroelec. Freq. Control **43** (1996) 303–311.

[32] S. Zeroug, L. B. Felsen: Non specular reflection of two- and three-dimensional acoustic beams from fluid-immersed plane-layered elastic structures. J. Acoust. Soc. Am. **95** (1994) 3075–3089.

[33] A. U. Rehman, C. Potel, J. F. de Belleval: Numerical modeling of the effects on reflected acoustic field for the changes in internal layer orientation of a composite. Ultrasonics **36** (1998) 343–348.

[34] C. Potel, S. Baly, J. F. De Belleval, M. Lowe, P. Gatignol: Deviation of a monochromatic lamb wave beam in anisotropic multilayered media: asymptotic analysis, numerical and experimental results. IEEE Trans. Ultrasonics Ferroel. Freq. Contr. **52** (2005) 987–1001.

[35] B. A. Auld: Acoustic fields and waves in solid. Wiley, New York, 1973.

[36] D. Royer, E. Dieulesaint: Elastic waves in solids. Vol 1: Free and guided propagation. Springer-Verlag, New York, 2000.

[37] A. Pilarski, J. L. Rose, K. Balasubramaniam: The angular and frequency characteristics of reflectivity from a solid layer embedded between two solids with imperfect boundary conditions. J. Acoust. Soc. Am. **87** (1990) 532–542.

[38] B. Vacossin, C. Potel, P. Gatignol, J. F. de Belleval: Interaction of a monochromatic ultrasonic beam with a finite length defect at the interface between two anisotropic layers - Kirchhoff approximation and Fourier representation. IEEE Trans. Ultrasonics Ferroel. Freq. Contr. submitted.

[39] J. B. Keller: Geometrical theory of diffraction. J. Opt. Soc. Am. **52** (1962) 116–130.

[40] J. S. Asvestas, R. E. Kleinman: The Strip. – In: Chapter 4 in: Electromagnetic and acoustic scattering by simple shapes (revised edition). J. J. Bowman, T. B. A. Senior, P. L. E. Uslenghi (eds.). Hemisphere Publishing Corporation, New York, 1987, ISBN 0–89116–885–0.